Zinc Oxide Prepared by Homogeneous Hydrolysis with Thioacetamide, Its Destruction of Warfare Agents, and Photocatalytic Activity

Vendula Houšková,*,†,‡ Václav Štengl,† Snejana Bakardjieva,† Nataliya Murafa,† Andrea Kalendová,‡ and Frantisek Opluštil§

Institute of Inorganic Chemistry, Academic of Sciences of the Czech Republic, Rez 250 68, Czech Republic, Faculty of Chemical Technology, Institute of Polymeric Materials, University of Pardubice, Nam. Cs. Legií 562, Pardubice 532 10, Czech Republic, and Military Technical Institute of Protection, Veslarska 230, Brno 628 00, Czech Republic

Received: February 1, 2007; In Final Form: March 1, 2007

Zinc sulfide (ZnS) nanoparticles were prepared by homogeneous hydrolysis of zinc sulfate and thioacetamide (TAA) at 80 °C. After annealing at a temperature above 400 °C in oxygen atmosphere, zinc oxide (ZnO) nanoparticles were obtained. The ZnS and ZnO nanoparticles were characterized by X-ray diffraction (XRD), scanning electron microscopy (SEM), high-resolution transmission electron microscopy (HRTEM), selected area electron diffraction (SAED), and Brunauer−Emmett−Teller (BET)/Barrett−Joyner−Halenda (BJH) methods were used for surface area and porosity determination. The photocatalytic activity of as-prepared zinc oxide samples was determined by decomposition of Orange II dye in aqueous solution under UV irradiation of 365 nm wavelength. Synthesized ZnO were evaluated for their non-photochemical degradation ability of chemical warfare agents to nontoxic products.

1. Introduction

Photocatalytic degradation processes have been widely applied as techniques of destruction of organic pollutants in wastewater and effluents. Titanium dioxide (TiO_2) has been extensively investigated as one of the most active semiconductor photocatalysts.[1] It has been known that ZnO is a suitable alternative to TiO_2 so far as band gap energy is concerned, and in fact higher photocatalytic efficiency compared with TiO_2 has been reported for ZnO.[2−4]

Homogeneous hydrolysis with urea as a precipitate agent can be used for preparation of oxo-compounds, such as metal oxides and hydroxides or precursor on base mixed oxo-hydroxides. The urea method is based on thermal decomposition of urea at a temperature higher than 60 °C.[5,6]

$$(NH_2)_2CO + 3H_2O \rightarrow CO_2\uparrow + 2NH_4OH \quad (1)$$

$$NH_4OH + H_2O \rightarrow NH_4^+ + OH^- \quad (2)$$

$$Me^{2+} + 2OH^- \rightarrow Me(OH)_2 \quad (3)$$

With heating of an aqueous solution of urea, the stoichiometry of urea hydrolysis can be described by

$$OC(NH_2)_2 + H^+ + 2H_2O \rightarrow HCO_3^- + 2NH_4^+ \quad (4)$$

According to Soler-Illia,[7] the hydrolysis of urea takes places in two steps:

$$OC(NH_2)_2 \rightarrow OCN^- + NH_4^+ \quad (5)$$

$$OCN^- + H^+ + 2H_2O \rightarrow HCO_3^- + NH_4^+ \quad (6)$$

The first step, the reversible formation of ammonium cyanate, is followed by the irreversible hydrolysis of cyanate ions. During the decomposition of urea, the NH_4^+ ions are formed and the consumption of H^+ results in an increase of pH in the solution. After reaching the pH value necessary for precipitation of the hydroxides, precipitates of insoluble material start to form.[7] Contrary to the heterogeneous precipitation method, when acidic metal salt solution is mixed with the basic neutralizing agent, much milder concentration gradients occur during the homogeneous precipitation, resulting in significantly different properties of the precipitation product.

Homogeneous precipitation in aqueous solution for preparation of spherical particles of ferrihydrite,[8,9] spherical particles of photocatalytic anatase,[10,11] nanosized anatase or ferrihydrite for decomposition of warfare agents,[12] and pigments based on mica coated with oxides of metal[13,14] was used.

In the same way as the urea method, homogeneous precipitation of metal sulfides by thermal decomposition of thioacetamide (TAA) can be used.[15] Thioacetamide at a temperature higher than 60 °C in acidic solution released hydrogen sulfide:

$$CH_3CSNH_2 + H_2O \rightarrow CH_3CONH_2 + H_2S \quad (7)$$

$$H_2S + H_2O \rightarrow HS^- + H_3O^+ \quad (8)$$

$$Me^{2+}HS^- \rightarrow MeS + H^+ \quad (9)$$

The reaction products are nanosized spherical particles with a well-developed microstructure, but different from homogeneous precipitation with urea. These products with high specific surface area are very well washed and filtered.

* To whom correspondence should be addressed. Telephone: 420 2 6617 3534. Fax.: 420 2 2094 0257. E-mail: houskova@iic.cas.cz.
† Academy of Sciences of the Czech Republic.
‡ Univesity of Pardubice.
§ Military Technical Institute of Protection.

10.1021/jp070878d CCC: $37.00
Published on Web 04/27/2007

According to Valenzuela and co-workers,[16] ZnO was prepared by precipitation of zinc(II) nitrate salts with an aqueous solution of NH_4OH. Calcined in static air at a temperature of 800 °C for 8 h and characterized by photodegradation of phenol. Ultrafine ZnO particles (12−25 nm) were prepared by thermal decomposition of zinc carbonate hydroxide.[17] ZnO particles were prepared that ranged from 5 to 12 nm from zinc acetate solution by the filter expansion aerosol generator (FEAG) process.[18] Flame spray pyrolysis, i.e., spray pyrolysis assisted with flame, was employed to synthesize spherical ZnO nanoparticles.[19] Photocatalytic decolorization of azo dye Orange II in water has been examined in an external UV light irradiation slurry photoreactor using zinc oxide[20] as a semiconductor photocatalyst. The paper[21] reports the large-scale synthesis of hexagonal cone-shaped ZnO nanoparticles by the esterification between zinc acetate and alcohol. The prepared ZnO particles exhibit high photocatalytic activity for the photocatalytic degradation of rhodamine B. The ZnO/ZnO_2 composites of photocatalysts were synthesized by hydrothermal treatment at 120−180 °C of ZnO_2, which in turn was obtained from an aqueous solution of $ZnSO_4$ and H_2O_2. The composite particles showed the morphology of ZnO prismatic crystallites with small ZnO_2 granules at the surface.[22] ZnO powders with different morphologies were synthesized by alkali precipitation, organozinc hydrolysis, and spray pyrolysis.[23] Acetaldehyde decomposition was used as a probe reaction to evaluate the photocatalysis of these ZnO powders. Thin zinc oxide[24] films with a thickness range from 10 to 80 nm have been grown on silicon substrates by the thermal physical vapor deposition approach. One paper[25] reports of the synthesis of self-assembled aligned hexagonal prismatic Cu-doped ZnO nanoparticles in aqueous and organic medium for photocatalytic hydrogen production under visible light irradiation.

The ability of nanodispersed metal oxides (MgO, CaO, ZnO, $AlO_x(OH)_y$, Al_2O_3, ZrO, and TiO_2, etc.) to decompose certain very toxic substances, such as sarine, somane, VX agent, or HD agent into nontoxic products was studied in detail by Wagner et al.[26,27] and Koper et al.[28] Reactivity with warfare agents of the nanosized MgO nanoparticles prepared in an autoclave hypercritical drying procedure from $Mg(OCH_3)$[29] and nanosized alumina (α-Al_2O_3)[30] from aluminum *sec*-butoxide was studied. Nanoparticles of iron and titanium oxides prepared by homogeneous hydrolysis of ferric sulfate and titanium oxosulfate[31] are used for decomposition of warfare agents.

In this study thioacetamide instead of urea was used as the precipitation agent in the synthesis of zinc sulfide, which is a precursor for preparing spherical clusters of zinc oxide nanoparticles. The photocatalytic activity on an Orange II dye and sulfur mustard non-photochemical decomposition on the prepared ZnO samples are tested.

2. Experimental Section

2.1. Synthesis of Samples. All used chemicals, zinc sulfate and thioacetamide (TAA), were analytical grade and were supplied by Fluka. A 1 M amount of $ZnSO_4 \cdot 7H_2O$ was dissolved in 4 L of distilled water, and 1 M thioacetamide was added. The reaction mixture was adjusted to pH = 2 with sulfuric acid. The reaction mixture was heated at temperature of 80 °C under stirring for 4 h. Thus-synthesized zinc sulfide was washed with distilled water with decantation, filtered off, and dried at 105 °C in furnace atmosphere. After annealing in the temperature range of 200−800 °C in oxygen atmosphere for 1 h, six fine ZnO/ZnS powders denoted as SIS 7_200, SIS 7_400, SIS 7_500, SIS 7_600, SIS 7_700, and SIS 7_800 were synthesized.

2.2. Characterization Methods. Surface areas of the samples were determined from nitrogen adsorption−desorption isotherms at liquid nitrogen temperature using a Coulter SA3100 instrument with outgas for 15 min at 120 °C. The Brunauer−Emmett−Teller (BET) method was used for surface area calculation;[32] the pore size distribution (pore diameter and pore volume of the samples) was determined by the Barrett−Joyner−Halenda (BJH) method.[33]

Transmission electron micrographs (TEM and HRTEM) were obtained by using two instruments, namely, Philips EM 201 operated at 80 kV and JEOL JEM 3010 operated at 300 kV (LaB6 cathode). Copper grid coated with a holey carbon support film was used to prepare samples for the TEM observation. A powdered sample was dispersed in ethanol, and the suspension was treated in an ultrasonic bath for 10 min.

Scanning electron microscopy (SEM) studies were performed using a Philips XL30 CP microscope equipped with energy-dispersive X-ray (EDX), Robinson, SE, and BSE detectors. The sample was placed on an adhesive C slice and coated with a 10 nm thick layer of Au−Pd alloy.

X-ray powder diffraction patterns were obtained on a Siemens D5005 instrument using Cu Kα radiation (40 kV, 30 mA) and diffracted beam monochromator. Qualitative analysis was performed with the Eva Application and the Xpert HighScore using the JCPDS PDF-2 database. Crystallite sizes of the samples were calculated from the Scherrer equation.[32]

Kinetics of the photocatalytic degradation as well as mineralization of 25 mL of 0.25 mM Orange II dye[34] and 200 mL solutions with particles of zinc oxide (200 mg/L) were measured. Quartz water-jacketed laboratory photoreactor, magnetically stirred and continuously irradiated with one "black light" lamp (λ = 365 nm, $I_0 = 5.3 \times 10^{-5}$ einstein dm^{-3} s^{-1}), was used. The laboratory irradiation experiments were performed in a self-constructed photoreactor. It consists of two coaxial quartz tubes placed in the middle of a steel cylinder with aluminum foil covering its inner wall. The inner quartz tube (diameter, 24 mm; length, 300 mm) was filled with the investigated suspension (70 mL) and magnetically stirred. Cooling water was circulating between the inner and the outer quartz tubes to keep a constant temperature of 20 °C. The used source of UV irradiation was a high-pressure mercury lamp enclosed in a glass filter bulb whose emission consists to 93% of 365 nm radiation. It was placed close to the quartz tubes. By means of the ferrioxalate actinometry, an average light intensity entering the volume of 50−70 mL of the irradiated solution was determined to be $I_0 = 5.3 \times 10^{-5}$ einstein dm^{-3} s^{-1}. The irradiated solution was sucked from the reactor with a peristaltic pump through a flow cuvette back to the reactor. The concentration of Orange II dye was determined by measuring the absorbance at 480 nm with visible spectrophotometer ColorQuestXE.

Prepared ZnO samples were evaluated for their ability to convert sulfur mustard (hereafter also signed as HD) into nontoxic products. Synthesized powdery samples were dried over 24 h in a vacuum kiln (at 100 °C, 400 Pa) before tests. A weighed portion of a given evaluated sample was put into a glass vial provided with a solid screw cap (Supelce, type CRS-33). The toxic agent in a solution of a chosen solvent was dosed onto the powder reagent layer. The vial was sealed with a cap and placed into the thermostat. All experiments were performed at 25 °C, and each run was repeated four to six times. An addition of isopropyl alcohol (2 mL) terminated the reaction. The suspension was vigorously agitated, and the liquid fraction was separated from the solid using a centrifuge (9000 cm^3 min^{-1} for 3 min) and subsequently analyzed for residual content of

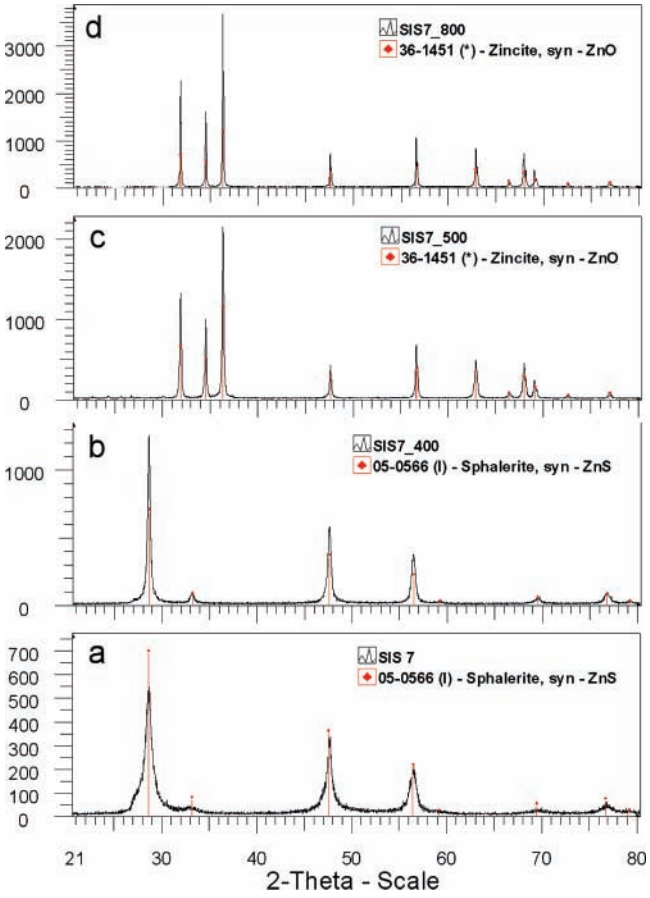

Figure 1. XRD patterns of the ZnS (a) and ZnS samples annealed at temperature of 400 (b), 500 (c), and 800 °C (d).

the mustard. The respective detoxification capabilities of the evaluated samples were expressed as percentages of mustard elimination from the reaction mixture under the given experimental condition.

3. Results and Discussion

3.1. X-ray Diffraction. The X-ray diffraction (XRD) pattern for sample SIS7 prepared by homogeneous hydrolysis of zinc(II) sulfate with TAA is shown in Figure 1a. It shows that the nanocrystals exhibit a zinc blende crystal structure (ZnS, PDF 05-0566).

It is known that a decrease in particle size results in a broadening of the diffraction peaks. From full-width at half-maximum (fwhm) of the strongest diffraction peak in plane (1 1 1), the mean particles size t in diameter was determined from the peak half-width B by Scherrer formula:[35]

$$t = \frac{k\lambda}{B\cos\Theta} \tag{10}$$

where k is a shape factor of the particle ($k = 1$ if the spherical shape is assumed) and λ and Θ are the wavelength and the incident angle of the X-rays, respectively. The peak width was measured at half of the maximum intensity. Parts b−d of Figure 1 show the XRD patterns of sample SIS7 annealed at the temperatures of 400, 500, and 800 °C in oxygen atmosphere. As is shown in XRD patterns, the zinc blende structure was transformed into zincite (ZnO, PDF 36-1451) at a temperature higher than 400 °C. It suggested that the zinc sulfide nanoparticles were oxidized into ZnO nanoparticles. According to eq 11 shown below, oxidation of ZnS occurred with the exchange reaction between oxygen and sulfur:

$$2ZnS + 3O_2 \rightarrow 2ZnO + 2SO_2\uparrow \tag{11}$$

In reference to Figure 1, the strongest diffraction peak in plane (1 0 1) consists of the standard zinc oxide powder diffraction file. From fwhm values of the zinc oxide (1 0 1) plane diffraction peak, the particle diameters were obtained. Table 1 shows the result calculated from the Debeye−Scherrer formula. In Table 1, we have found that the particle size (t) increases with the increasing annealing temperature.

3.2. Surface Area and Porosity. In Table 1 is shown the surface area (BET), the pore distribution, and the total volume of pores related to mass (porosity) of samples obtained at various heating temperatures.

These results show that the specific surface of zinc sulfide (samples SIS7 and SIS7_200) grow with increased temperature. At a temperature of 400 °C (sample SIS7_400) a recrystallization process take place and the specific surface area is decreased. With increasing temperature above 400 °C (samples SIS7_500−SIS7_800) the specific surface area decreases.

The pore distribution calculated from the BJH method confirms that zinc sulfide and zinc oxide samples are microporous with pore sizes in the range of 2−6 nm. Variable annealing temperature did not change the total pore area and the total pore volume (Table 1).

3.3. High-Resolution Transmission Electron Microscopy and Electron Diffraction. Image processing analysis of a HRTEM micrograph is a useful method in the refinement of a microstructure in the sense that we can more accurately analyze grain sizes and grain boundaries. Furthermore, from fast Fourier transform (FFT) it is possible to determine and to index crystallographic planes and find orientations of nanoparticles. Figure 2 shows HRTEM micrographs of zinc sulfide (sphalerite) particles, prepared by homogeneous precipitation with thioacetamide. Figure 2d shows that the lattice spacing of approximately 0.347 nm between adjacent lattice planes corresponds to the distance between 200 crystal planes. As it follows from a database (PDF 05-0566, JCPDS PDF2, 2001), the lattice spacing 0.347 corresponds to the 200 diffraction line of sphalerite.

HRTEM images of ZnO crystallites (see Figure 3) obtained at annealing sample SIS 7 at a temperature of 700 °C in oxygen atmosphere (sample SIS7_700) shows two types of domains corresponding to ZnO space group $Fm\bar{3}m$. The face-centered

TABLE 1: Characteristics of Prepared Samples

sample	heating temp (°C)	RTG	t (nm)	BET ($m^2\ g^{-1}$)	total pore area (nm)	total pore vol ($cm^3\ g^{-1}$)	K (min^{-1})
SIS7	0	ZnS	6.2	76.8	1.718	0.02	
SIS7_200	200	ZnS	18.0	153.5	1.536	0.06	
SIS7_400	400	ZnS	19.9	101.9	1.527	0.01	0.0005
SIS7_500	500	ZnO	41.8	50.54	1.530	0.02	0.0043
SIS7_600	600	ZnO	48.7	35.9	1.527	0.01	0.0079
SIS7_700	700	ZnO	74.2	31.3	1.527	0.01	0.0379
SIS7_800	800	ZnO	75.9	13.4	1.527	0.01	0.0196
Deggusa P25		TiO_2		50			0.0222

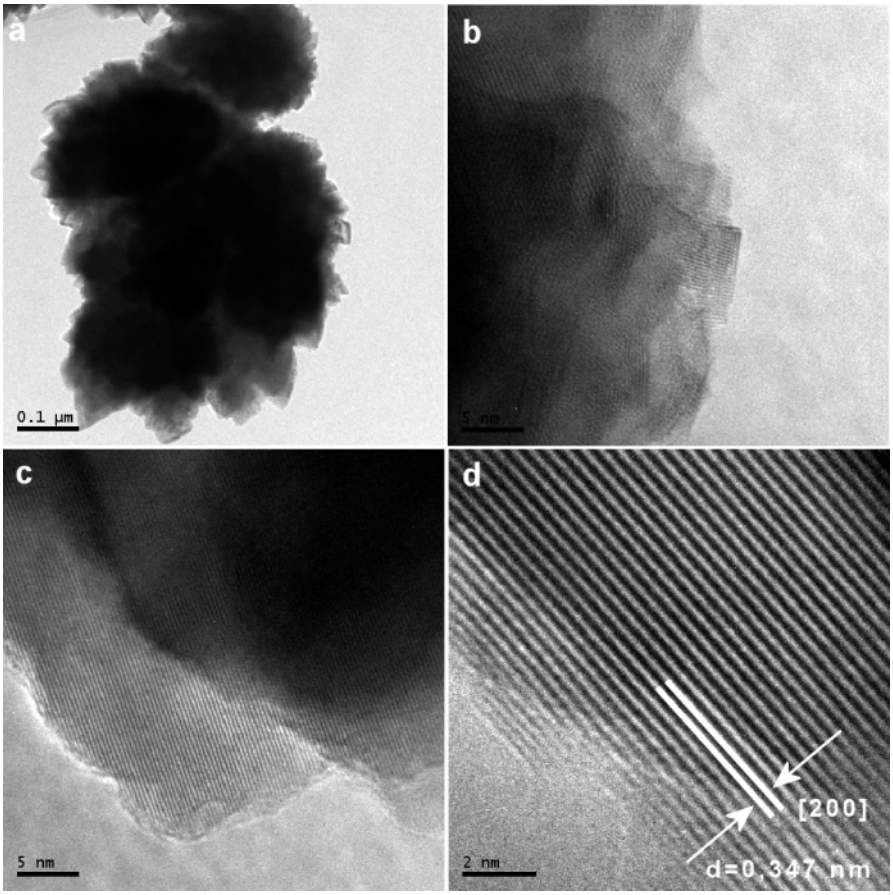

Figure 2. HRTEM micrographs of sphalerite prepared by homogeneous precipitation with TAA denoted as SIS7 (magnification 25 000).

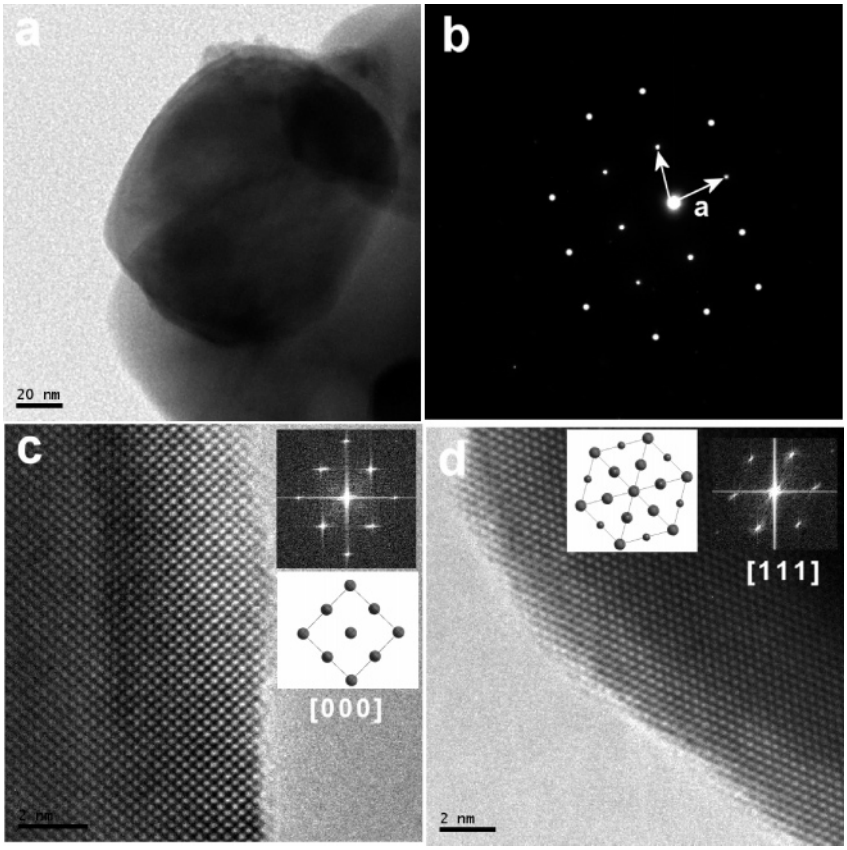

Figure 3. HRTEM micrographs of zincite prepared by annealing of the sample denoted as SIS7 at a temperature of 600 °C for 2 h in oxygen atmosphere (magnification 100 000).

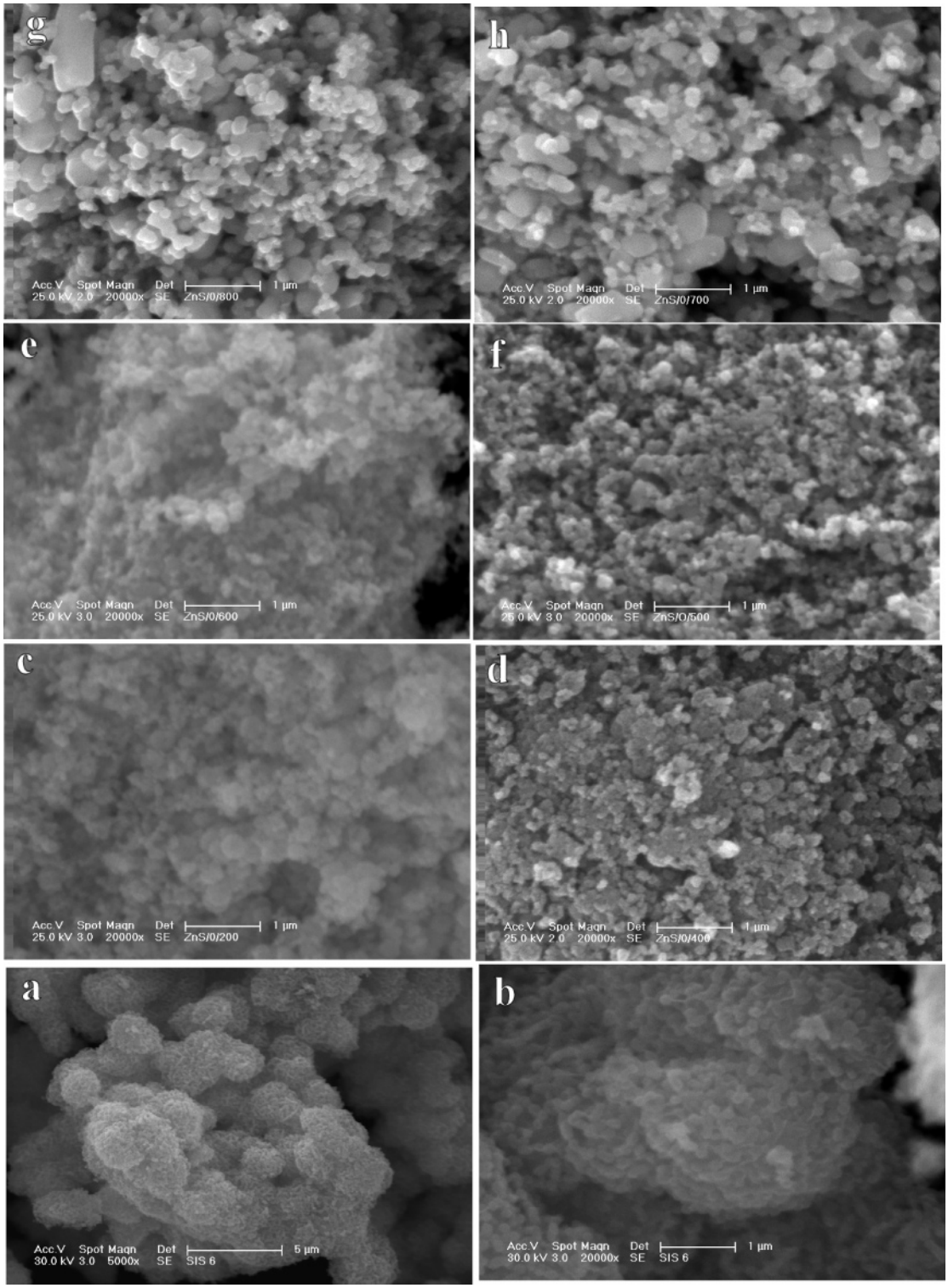

Figure 4. SEM micrographs of particles prepared by homogeneous hydrolysis of zinc sulfate and thioacetamide (TAA) at a temperature of 80 °C (a,b) and SEM micrographs after annealing at 200 (c), 400 (d), 500 (f), 600 (e), 700 (h), and 800 °C (g).

cubic unit cell has been used to index the electron diffraction (ED) pattern (calculated by FFT) inserted in Figure 3. The motive on Figure 3c corresponding to plane 001 and the motive on Figure 3d correspond to plane 111. Figure 3b depicts the corresponding selected area of electron diffraction pattern (SAED). The particle size calculated from HRTEM is similar to that obtained from X-ray powder diffraction method.

3.4. Scanning Electron Microscopy. It is apparent that the product of homogeneous precipitation of thioacetamide and zinc sulfate consists of approximately spherical round particles, agglomerates of diameter of about 1 μm (Figure 4a,b), which are formed from spherical particles of 6 nm joined to the chains. After oxidation, agglomerates and chains of particles have disintegrated and a particle cluster of approximately size of 10 nm has been formed. With increasing annealing temperature, the agglomerate size decreases (Figure 4c−h).

3.5. Photocatalytic Activity. The photocatalytic activity of as-prepared samples was determined by degradation of Orange II dye aqueous solutions under UV radiation. In regions where Lambert−Beer law (12) is significant, the concentration is

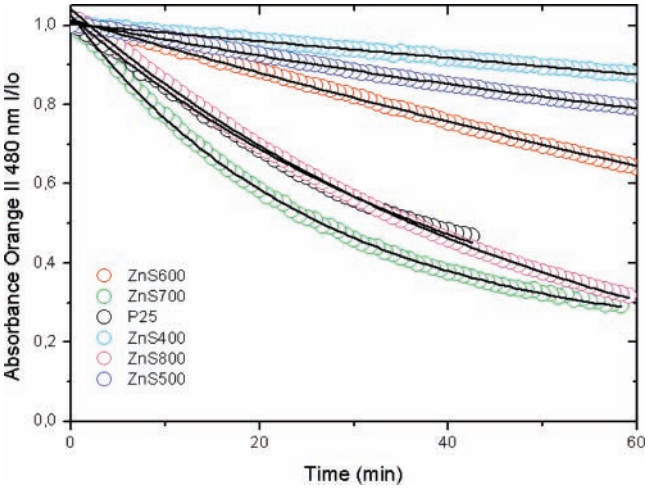

Figure 5. Photocatalytic decomposition of Orange II dye on zinc sulfide (ZnS) samples annealed at a temperature above 400 °C (SIS7_400−800) and on the standard photocatalyst Degussa (P25). Absorbance is expressed as I/I_0, where I is the intensity of absorbance at 480 nm of solution containing sample and Orange II dye in real time and I_0 is the intensity of absorbance at 480 nm of the initial solution of sample and Orange II dye.

proportional to absorbance

$$A = \epsilon c l \tag{12}$$

where A is absorbance, c is the concentration of the absorbing component, l is the length of the absorbing layer, and ϵ is the molar absorbing coefficient. The time dependences of Orange II dye decomposition can be described by using eq 13 for the first kinetics reaction:[36]

$$\frac{\mathrm{d[OII]}}{\mathrm{d}t} = k(a_0 - [\mathrm{OII}]) \tag{13}$$

where [OII] is the concentration of Orange II dye, a_0 is the initial concentration of Orange II dye, and k is the rate constant. It is obvious from Figure 5 that the first-order kinetics curves (plotted as lines) fitted to all experimental points.

In fact, illumination of the surface of zincite by photons of energy greater than the band gap energy (3 eV) creates a pair of electron e^- and holes h^+ following the reaction

$$\mathrm{ZnO} + h\nu \rightarrow \mathrm{ZnO}(e^-, h^+) \tag{14}$$

The valence band photogenerated holes are free to react with OH^- adsorbed onto the surface of ZnO to create hydroxyl radicals $OH^\bullet$. The band electrons react with electron acceptors such as oxygen creating oxygen radicals $O_2^{\bullet -}$.[34]

These radicals present extremely strong oxidizing properties and are able to degrade the Orange II dye entirely to water and carbon dioxide:

$$OH^\bullet + O_2^{\bullet -} + \mathrm{OII} \rightarrow \text{intermediates} \rightarrow CO_2 + H_2O \tag{15}$$

The photocatalytic degradation of Orange II dye is presented in Figure 5 and Table 1. The zincite particles show good photocatalytic properties for the decomposition of Orange II dye in an aqueous solution under UV radiation.

On the basis of the results in Table 1, we have found that the rate constant k of the mineralization of Orange II dye increases with annealing temperature. Probably, well-crystallized nanoparticles with average size of 40−75 nm and with perfect crystal structure improve the photocatalytic activity of ZnO particles. The corresponding kinetic curve of the standard photocatalyst P25 (Degussa) is included.

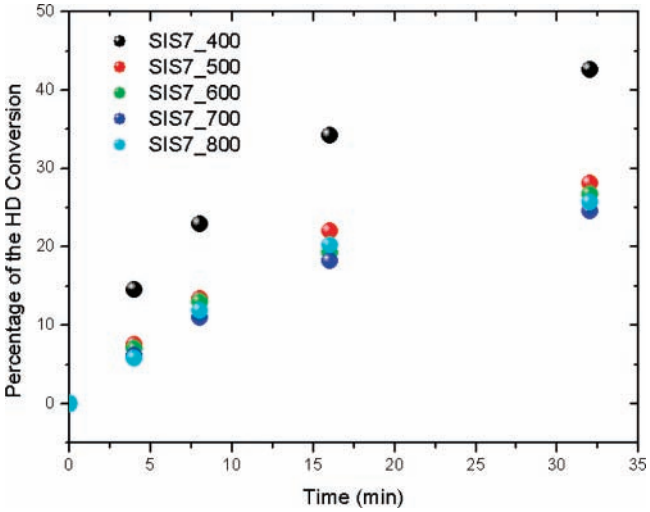

Figure 6. Decomposition of sulfur mustard on prepared samples with time.

3.6. Method of Disintegration of Warfare Agents. The testing of the detoxification activity of prepared mixed oxides was made with the use of mustard gas. Mustard gas was taken purposely because it is the most resistant among standard chemical agents against nanodispersive oxides. Reaction schemes of non-photochemical destruction of sulfur mustard were described by Wagner and co-workers.[26,27,36]

The samples of zinc oxide were evaluated for their ability to degrade chemical warfare agents (sulfur mustard gas) to nontoxic products. The respective detoxification capabilities of evaluated samples were expressed as percentages of the sulfur mustard HD conversion (see Figure 6). Good results were obtained by the decomposition on zinc oxide annealed at temperature of 400 °C (sample SIS7_400), where conversion comes to 42%. Increasing the annealing temperature decreases the non-photochemical decomposition of warfare agents due to the lower specific surface area of the samples.

4. Conclusion

The spherical particles of zinc sulfide were prepared by homogeneous hydrolysis of zinc(II) sulfate in aqueous solution at a temperature of 60 °C with thioacetamide. The ZnS was annealed in oxygen atmosphere in a temperature range of 200−800 °C and converted to ZnO.

The solids consisted of uniform spherical aggregates with a diameter of approximately 1 μm.

The photocatalytic activity of as-prepared zinc oxide samples was determined by decomposition of Orange II dye in aqueous solution under UV irradiation of 365 nm wavelength The sample heated at a temperature of 700 °C exhibited a good photocatalytic activity, $k = 0.0379\ \mathrm{min}^{-1}$. ($k$ for P25 Degussa is 0.0222 min^{-1}.)

Nanosized anatase and ferrihydrite prepared by homogeneous hydrolysis with urea efficiently decompose chemical warfare agents such as mustard gas, soman, and VX.[31] Sample ZnO prepared by homogeneous hydrolysis with thioacetamide heated at a temperature of 400 °C established a good decomposition of the mustard gas, and its reactivity is superior to AP−MgO.[26]

Acknowledgment. The work was supported by the Academy of Sciences of the Czech Republic (Project No. AV0Z40320502).

References and Notes

(1) Fujishima, A.; Rao, T. N.; Tryk, D. A. *J. Photochem. Photobiol., C* **2000**, *1*, 1.

(2) Liao, S.; Donggen, H.; Yu, D.; Su, Y.; Juan, G. *J. Photochem. Photobiol., A* **2004**, *168*, 7.

(3) Khodja, A. A.; Sehili, T.; Pilichowski, J. F.; Boule, P. *J. Photochem. Photobiol., A* **2001**, *141*, 231.

(4) Lizama, C.; Freer, J.; Baeza, J.; Mansilla, H. D. *Catal. Today* **2002**, *76*, 235.

(5) Ocana, M.; Morales, M. P.; Serna, C. J. *J. Colloid Interface Sci.* **1998**, *212*, 317.

(6) Song, K. Ch.; Kang, Y. *Mater. Lett.* **2000**, *42*, 283.

(7) Soler-Illia, G.; Jobbagy, M.; Candal, R. J.; Regazzoni, A. E.; Blesa, M. A. *J. Dispersion Sci. Technol.* **1998**, *19*, 207.

(8) Šubrt, J.; Boháček, J.; Štengl, V.; Grygar, T.; Bezdička, P. *Mater. Res. Bull.* **1999**, *34*, 905.

(9) Bakardjieva, S.; Štengl, V.; Šubrt, J.; Večerníková, E. *Solid State Sci.* **2005**, *7* (4), 367.

(10) Bakardjieva, S.; Šubrt, J.; Štengl, V.; Dianez, M. J.; Sayagues, M. J. *Appl. Catal., B* **2005**, *58* (3−4), 193.

(11) Štengl, V.; Šubrt, J.; Bezdička, P.; Maříková, M.; Bakardjieva, S. *Solid State Phenom. V* **2003**, *121*, 90−91.

(12) Štengl, V.; Maříková, M.; Bakardjieva, S.; Šubrt, J.; Opluštil, F.; Olšanská, M. *J. Chem. Technol. Biotechnol.* **2005**, *80* (7), 754.

(13) Štengl, V.; Šubrt, J.; Bakardjieva, S.; Kalendová, A.; Kalenda, P. *Dyes Pigm.* **2003**, *58* (3), 239.

(14) Štengl, V.; Šubrt, J.; Bakardjieva, S.; Bezdička, P.; Kalendová, A.; Kalenda, P. *Solid State Chem. V* **2003**, *115*, 90−91.

(15) Nomura, T.; Kousaka, Y.; Alonso, M.; Fukunaga, M. *J. Colloid Interface Sci.* **2000**, *223*, 179.

(16) Valenzuela, M. A.; Bosch, P.; Jiménez-Becerrill, J.; Quiroz, O.; Páez, A. I. *J. Photochem. Photobiol., A* **2002**, *148*, 177.

(17) Jing, L.; Xu, Z.; Sun, X.; Shang, J.; Cai, W. *Appl. Surf. Sci.* **2001**, 180, 308.

(18) Park, S. B.; Kang, Y. C. *J. Aerosol Sci.* **1997**, *28*, 473.

(19) Jang, Y. J.; Simer, C.; Ohm, T. *Mat. Res. Bull.* **2006**, *41*, 67.

(20) Nishio, J.; Tokumura, M.; Znad, H. T.; Kawase, Y. *J. Hazard. Mater.* **2006**, *138*, 106.

(21) Ren, X.; Han, D.; Chen, D.; Tang, F. *Mat. Res. Bull.*, in press.

(22) Hsu, C. C.; Wu, N. L. *J. Photochem. Photobiol., A* **2005**, *172*, 269.

(23) Haneda, D.; Li, H. *Chemosphere* **2003**, *51*, 129.

(24) Fouad, O. A.; Ismail, A. A.; Zaki, Z. I.; Mohamed, R. M. *Appl. Catal., B* **2006**, *62*, 144.

(25) Kanade, K. G.; Kale, B. B.; Baeg, J.; Lee, S. M.; Lee, C. W.; Moon, S.; Chang, H. *Mat. Chem. Phys.*, in press.

(26) Wagner, G. W.; Bartram, P. W.; Koper, O.; Klabunde, K. J. *J. Phys. Chem. B* **1999**, *103*, 3225.

(27) Wagner, G. W.; Procell, L. R.; O'Connor, R. J.; Munavalli, S.; Cannes, C. L.; Kapoor, P. N.; Klabunde, K. J. *J. Am. Chem. Soc.* **2001**, *123*, 1636

(28) Koper, O.; Lucas, E.; Klabunde, K. J. *J. Appl. Toxicol.* **1999**, *19*, 59.

(29) Štengl, V.; Bakardjieva, S.; Maříková, M.; Šubrt, J.; Opluštil, F.; Olšanská, M. *J. Chem.* **2004**, *1*, 1.

(30) Štengl, V.; Bakardjieva, S.; Maříková, M.; Šubrt, J.; Opluštil, F.; Olšanská, M. *Ceramics* **2003**, *47*, 175.

(31) Štengl, V.; Marikova, M.; Bakardjieva, S.; Šubrt, J. *J. Chem. Technol. Biotechnol.* **2005**, *80*, 754.

(32) Brunauer, S.; Emmett, P. H.; Teller, E. *J. Am. Chem. Soc.* **1938**, *60*, 309.

(33) Barret, E. P.; Joyner, L. G.; Halenda, P. P. *J. Am. Chem. Soc.* **1951**, *73*, 373.

(34) Stylidi, M.; Kondarides, D. I.; Verykios, X. E. *Appl. Catal., B* **2004**, *47*, 189.

(35) Patterson, A. L. *Phys. Rev.* **1939**, *56*, 978.

(36) Macounová, K.; Krýsová, H.; Ludvík, J.; Jirkovský, J. *J. Photochem. Photobiol., A* **2003**, *156*, 273.

(37) Wagner, **G**. W.; Koper, O. B.; Lucas, E.; Decker, S.; Klabunde, K. J. *J. Phys. Chem. B* **2000**, *104*, 5118.